Modulation of Photo Induced Iodine Expulsion in Mixed Halide Perovskites with Electrochemical Bias

Jeffrey T. DuBose[1,2,#] Preethi S. Mathew[1,2,#] Junsang Cho[1], Masaru Kuno[2] and Prashant V. Kamat[1,2,3*]

[1]Notre Dame Radiation Laboratory, [2]Department of Chemistry and Biochemistry, and [3]Department of Chemical and Biomolecular Engineering.
University of Notre Dame, Notre Dame, Indiana 46556, United States

---

# Equal contribution

* Address correspondence to this author pkamat@nd.edu

Hole trapping at I-sites in mixed halide perovskites (MHP) is responsible for iodine migration and its eventual expulsion into solution. We have now modulated the photoinduced iodine expulsion in MHP through externally applied electrochemical bias. At anodic potentials, electron extraction at TiO_2/MHP interfaces becomes efficient, leading to hole build-up within MHP films. This improved charge separation, in turn, favors iodine migration as evident from the increased apparent rate constant of iodine expulsion ($k_{expulsion}$ = 0.0030 s^{-1}). Conversely, at negative potentials (-0.3 V *vs.* Ag/AgCl) electron-hole recombination is facilitated within MHP, slowing down iodine expulsion by an order of magnitude ($k_{expulsion}$ = 0.00018 s^{-1}). The tuning of the E_{Fermi} level through external bias modulates electron extraction at the TiO_2/MHP interface, and indirectly controlling the build-up of holes, ultimately inducing iodine migration/expulsion. Suppressing iodine migration in perovskite solar cells is important for attaining greater stability since they operate under internal electrical bias.

TOC graphics

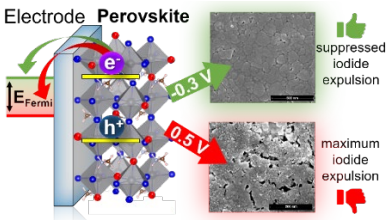

In mixed halide perovskites (MHPs) such as $APbBr_{3-x}I_x$ or $APbBr_{3-x}Cl_x$ (A is a cation, *e.g.*, Cs^+ or methylammonium), halide ion mobility leads to light-induced and field-induced segregation into distinct halide-rich phases.[1-6] Such photoinduced halide segregation negatively impacts the stability and efficiency of devices as iodide-rich domains act as charge recombination centers, greatly diminishing the performance of solar cells[7,8] and light emitting diodes.[9] Interestingly, the entropy of mixing favors the mixed halide phase in the dark.[10] A threshold excitation energy is needed to overcome this entropy of mixing to induce phase segregation.[11,12] Upon stopping photoirradiation, the segregated phases remix to restore the homogeneous starting composition. These compositional changes which can be readily monitored through optical changes (e.g., absorption and emission spectra) in the mixed halide film thus enable direct tracking of the halide ion movement.[13] These methods have given insights into the mobility of halide ions in physically paired 3D and 2D perovskites.[14-16]

The mobility of iodide in mixed halide perovskite films can lead to its expulsion under long term irradiation, thus inducing instability.[17-20] This photoinduced iodide expulsion can be readily seen upon irradiating perovskite films in contact with a solvent (such as DCM or toluene).[18] The selective removal of iodide from MHPs upon continued irradiation transforms the perovskite film into a bromide-rich phase. It was also shown that substituting the MHP A-site cation with cesium (Cs) slows down iodide expulsion due to increased thermodynamic stabilization of MHP lattices. [18,21,22] Similar lattice stabilization has been shown to reduce phase segregation in Cl-alloyed perovskites.[15,23,24] Surface treatments, and 2D interfaces have suppressed halide ion migration to some extent.[14,25-27] Such strategies provide a compositional means of modifying the energy barrier for halide segregation/expulsion. While most of the spectroscopic studies of halide ion migration are focused on the faster time scale measurements, the longer time scale migration studies are needed to elucidate its impact on the overall photostability.

Of note is a spectroelectrochemical approach, which has been used to determine the conduction and valence band positions of mixed halide perovskites and which has revealed their dependence on halide composition.[28,29] The control of defect densities in $CsPbBr_3$ films through externally applied bias has been shown to modulate the emission intensity.[30] Our recent success in maintaining MHP stability in dichloromethane (DCM) has enabled electrochemical and spectroelectrochemical studies to probe relevant charge transfer processes at perovskite/liquid interfaces.[31,32] We have now utilized spectroelectrochemical measurements to systematically vary the driving force for charge separation by modulating Fermi level through external bias and monitor its influence on halide ion migration. The macroscopic tracking of iodine migration under applied bias sheds new insights into degradation pathways.

Photoirradiation of Dry versus *Electrolyte-Contacting Perovskite Films.* When mixed halide perovskites (e.g. $MAPbBr_{1.5}I_{1.5}$) are subjected to continuous photoirradiation (above gap), they phase segregate into Br- and I-rich regions.[1,2]. An increase in absorbance in the red (~675 nm) indicates new absorption arising from the formation of iodide-rich domains, with a concomitant decrease in absorbance around ~625 nm due to depletion of the mixed phase (Figure S1A; Reactions 1 and 2).

$$MAPbBr_{1.5}I_{1.5} + h\nu \rightarrow MAPbBr_{1.5}I_{1.5}\ (e + h^+) \rightarrow MAPbBr_{1.5}I_{1.5} \quad (1)$$

$$MAPbBr_{1.5}I_{1.5}\ (e + h^+) \rightarrow \tfrac{1}{2}\ MAPbBr_3 + \tfrac{1}{2}MAPbI_3 \quad (2)$$

Upon stopping photoirradiation, segregated regions re-mix to attain entropic stabilization (Figure S1B).

Interestingly, when perovskite films are in contact with a solvent or electrolyte a continuous blue-shift of the band edge absorbance during steady state photoirradiation is observed, due to selective expulsion of iodine species into the solvent (reaction 5).[18] The sequence of reactions 3-5 are facilitated by the TiO_2 as it captures electrons thus accumulating holes in the film. The accumulated holes contribute to both photoinduced phase segregation as well as iodine expulsion.[4,18]

$$MAPbBr_{1.5}I_{1.5}(e^-,h^+) + TiO_2 \longrightarrow MAPbBr_{1.5}I_{1.5}(h^+) + TiO_2\,(e^-) \quad (3)$$

$$TiO_2\,(e^-) + FTO \longrightarrow TiO_2 + FTO\ (e^-) \quad (4)$$

$$2MAPbBr_{1.5}I_{1.5} + h^+ \rightarrow MAPbBr_3 + PbI_2 + MA^+ + \tfrac{1}{2}I_2 \quad (5)$$

Figure S2A shows the absorbance of a $MAPbBr_{1.5}I_{1.5}$ film in contact with 0.01 M tetrabutylammonium hexafluorophosphate (Bu_4NPF_6) in dichloromethane (DCM). Whereas a dry perovskite film (no solvent or electrolyte) segregates into Br- and I-rich domains, the perovskite film in contact with the electrolyte expels iodine into the solution (Figure S2B). As discussed in our previous study, Cs-alloying of $MAPbBr_{1.5}I_{1.5}$ films slows down iodide migration and reveals the formation of a phase segregated state prior to iodine expulsion.[18] This strategy of A-site cation modification greatly suppresses the thermodynamics of iodide expulsion.

Stable Electrochemical Window for Mixed Halide Perovskite. To investigate the effect of externally applied bias (and thus E_{Fermi}) on the photo-induced iodide expulsion process, we first established a stable electrochemical working window in which no Faradaic processes occur (i.e. no electrochemically-induced redox events) in dark. Films of $MAPbBr_{1.5}I_{1.5}$ were deposited onto TiO_2-coated FTO (fluorine doped tin oxide) electrodes using previously reported methods.[4] TiO_2 is used as an electron transport layer (ETL) in perovskite solar cells and was thus selected for this study. The resultant FTO/TiO_2/$MAPbBr_{1.5}I_{1.5}$ films were immersed in 0.01 M Bu_4NPF_6 in DCM, and electrochemical experiments were performed under degassed conditions (N_2 was pre-bubbled through DCM to reduce solvent loss).[31,32]

During this reduction scan (Figure 1A), we can clearly see a large decrease in absorbance of the perovskite due to the reduction of Pb to Pb^0 (-0.77 V). Similarly, when we scanned the potential in the positive direction (Figure 1B) we could see a distinct feature corresponding to the oxidation of the halide ions ~ 1 V. The absence of a Faradaic current and no loss in the absorbance within the electrochemical window, -0.3 V and +0.5 V (shaded regions in Figures 1A,B), ensured that we could control the E_{Fermi} of the electrode without inducing an electrochemical reaction at the perovskite-electrolyte interface. To confirm

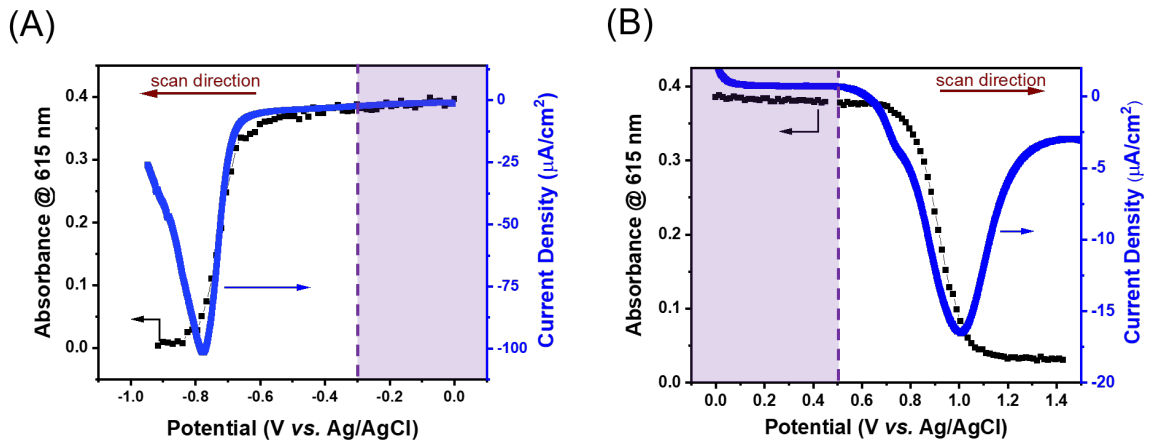

Figure 1: Spectroelectrochemcial data for FTO/TiO_2/$MAPbBr_{1.5}I_{1.5}$ films (0.5 mV/s sweep rate), during the (A) reduction and (B) oxidation half cycle together with the absorbance change at the excitonic peak (615 nm). The shaded region in each trace represent the stable window in which no Faradaic processes occur. Measurements were performed in 0.01 M Bu_4NPF_6 in DCM, under degassed N_2 conditions (pre-bubbled through DCM).

the stability of our perovskite films in this potential window over longer times, we recorded absorbance spectra of the films held at select bias potentials for 60 minutes in the dark (Figures S3 and S4).

Photo-induced Iodide Expulsion under Applied Bias. The set-up employed for spectroelectrochemical measurements is shown in Scheme S1 (SI). The absorbance spectra of MHP films at 3 different bias potentials (Figures 2A-C) within the stable electrochemical window were recorded during irradiation with a 405 nm CW diode laser (50 mW/cm^2). Changes in absorbance during iodide expulsion are better visualized through difference absorbance spectra (Figures 2D-F). In each case, a loss of absorbance is seen throughout the $MAPbBr_{1.5}I_{1.5}$ absorbance window, with a distinct bleach (negative) feature near 625 nm (excitonic peak of $MAPbBr_{1.5}I_{1.5}$). The absorbance loss and concurrent blue shift in the spectrum is associated with charge separation followed by iodine expulsion (Reaction 1-5).[32]

When the applied potential was maintained at 0.5 V, photoinduced iodine expulsion was rapid and complete within 15 minutes (Figure 2A,D). At 0 V *vs.* Ag/AgCl, we observe a relatively slower iodine expulsion process (Figure 2B,E). Even after 60 minutes of irradiation, films retain a small absorption feature around 615 nm, indicating incomplete expulsion of iodine from films. For a film held at an applied bias of -0.3 V *vs.* Ag/AgCl only a small change in absorption is seen (Figure 2C,F). This slower expulsion at cathodic potential indicates that the iodine migration becomes less efficient and only a small amount of iodine

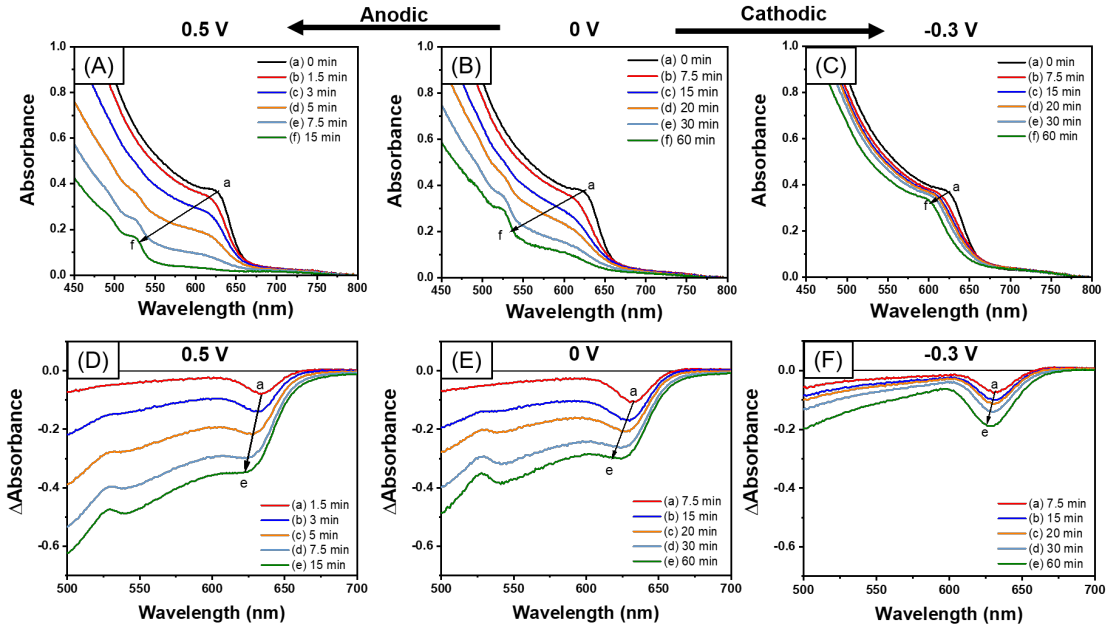

Figure 2: Absorbance spectra of FTO/TiO_2/$MAPbBr_{1.5}I_{1.5}$ films during 405 nm CW photoirradiation (50 mW/cm^2) while held at an applied bias of (A) 0.5 V, (B) 0 V, and (C) -0.3 V *vs.* Ag/AgCl. (D-F) Corresponding ΔAbsorbance graphs for each applied bias, which highlights the loss of absorbance (bleach) near 625 nm. Data for all applied biases are shown in the Supporting Information. Measurements were performed in 0.01 M Bu_4NPF_6 in DCM, under degassed N_2 conditions (pre-bubbled through DCM).

escapes from the film into the solution (absorption spectra of the electrolyte solution at these applied biases are shown in Figure S5). We have estimated the quantum efficiency of iodine expulsion based on the solution absorbance of I_3^- and incident laser power. The quantum efficiency for iodine expulsion was 0.042% at 0.5 V and 0.0044% at –0.3 V and agreed with the trend observed in Figure 2 (See Supporting Information for quantum efficiency measurements).

The absorbance and corresponding difference absorbance spectra of photoirradiated MHP films at other applied potentials (between +0.5 and -0.3 V *vs.* Ag/AgCl) are shown in Figures S6-9. The absorbance loss at 625 nm, which represents disappearance of MHP, was recorded at different times to obtain iodide expulsion kinetics (Figure 3A and S10). Each trace was fit to a monoexponential decay to determine the apparent rate constants of iodine expulsion. At 0.5 V *vs.* Ag/AgCl, the apparent rate constant, $k_{expulsion}$, was determined to be 0.003 s^{-1} and is an order of magnitude greater than the one observed at cathodic potentials ($k_{expulsion}$ = 0.00018 s^{-1} at -0.3 V). The dependence of apparent rate constant of photoinduced iodine expulsion on the applied potential is shown in Figure 3B. At potentials more negative than 0 V *vs.* Ag/AgCl, $k_{expulsion}$ remains unaffected. However, with increase in the applied potential (greater than 0 V), we observe an increase in $k_{expulsion}$. It is interesting to note that the electrochemical bias applied to the TiO_2/MHP film influences the photoinduced migration of iodine and ultimate expulsion of iodine. This further confirms our ability to modulate photoinduced migration of iodine in the MHP film through externally applied electrochemical bias.

Previously we have shown that an excitation intensity threshold exists for light-induced halide

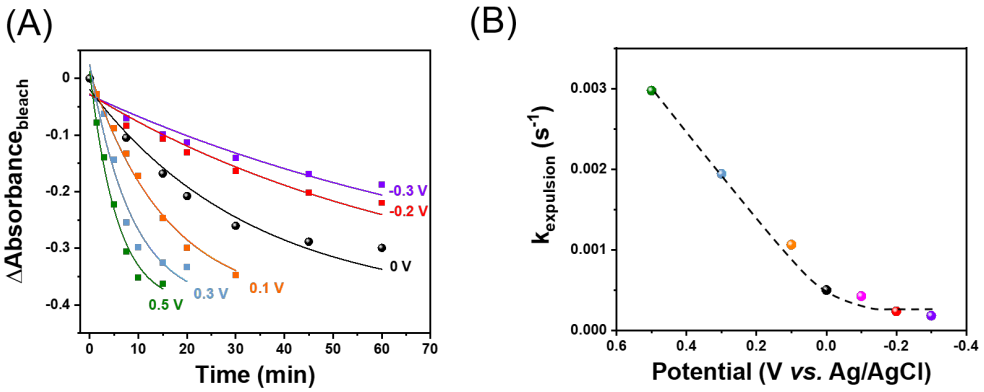

Figure 3: (A) Monoexponential fits to the differential absorbance bleach feature (625 nm) for FTO/TiO_2/$MAPbBr_{1.5}I_{1.5}$ films photoirradiated and held at potentials ranging from 0.5 to -0.3 V *vs.* Ag/AgCl. Data for all applied biases are shown in the Supporting Information. (B) The dependence of apparent rate constant of iodide expulsion ($k_{expulsion}$) determined from monoexponential fits in (A) on the applied potential. The dashed line is meant to guide the eye.

segregation[11,12,15,33]. A thermodynamic balance between the driving force for halide segregation (which is proportional to light intensity) and the entropy of mixing dictates the interaction. We found that iodide expulsion from films held at different potentials exhibits a similar excitation intensity threshold. Details of the threshold intensity determination can be found in the Supporting Information and individual absorbance spectra are shown in Figure S11. At 0.5 V *vs.* Ag/AgCl the $I_{Threshold}$ was lowest (~65 μW/cm^2). As the E_{Fermi} is raised by applying a more cathodic potential, the threshold intensity required to observe iodine expulsion increases four fold for cathodic potentials 0 and -0.3 V *vs.* Ag/AgCl, respectively (~290 μW/cm^2; Figure S12).

Photoelectrochemical Response of $MAPbBr_{1.5}I_{1.5}$ Films on FTO/TiO_2 Electrode. Another way to confirm the applied potential dependence of charge transfer processes is to probe photocurrent generation at perovskite/liquid interfaces.[34-36] A photocurrent density of ~5 μA/cm^2 is generated when the FTO/TiO_2/$MAPbBr_{1.5}I_{1.5}$ films are irradiated in a photoelectrochemical cell (Figure 4A). Due to a lack of redox couple present in this set-up, the observed photocurrent is relatively low. Following bandgap excitation, electrons from $MAPbBr_{1.5}I_{1.5}$ are quickly transferred to TiO_2 (Reaction 3) due to its favorably aligned conduction band.[4,37,38] These electrons are extracted into the FTO electrode (Reaction 4) to generate a photocurrent. The J-V characteristics in Figure 4 of the FTO/TiO_2/$MAPbBr_{1.5}I_{1.5}$ films under (a) dark and (b) 405 nm CW irradiation (50 mW/cm^2) show n-type semiconductor behavior. Thus, the applied bias directly dictates the Fermi level of the perovskite film and in turn charge separation within the space charge layer.

The application of external bias in the potential range -0.3 to +0.5 V affects the charge separation in the perovskite film, shifting the apparent Fermi level (E_{Fermi}) of the electrode either closer to or away from the TiO_2 conduction band. Figures 4B and C illustrate the photoinduced charge separation and the interfacial charge transfer under the influence of an external bias. At positive bias (*e.g.*, +0.5 V *vs.* Ag/AgCl),

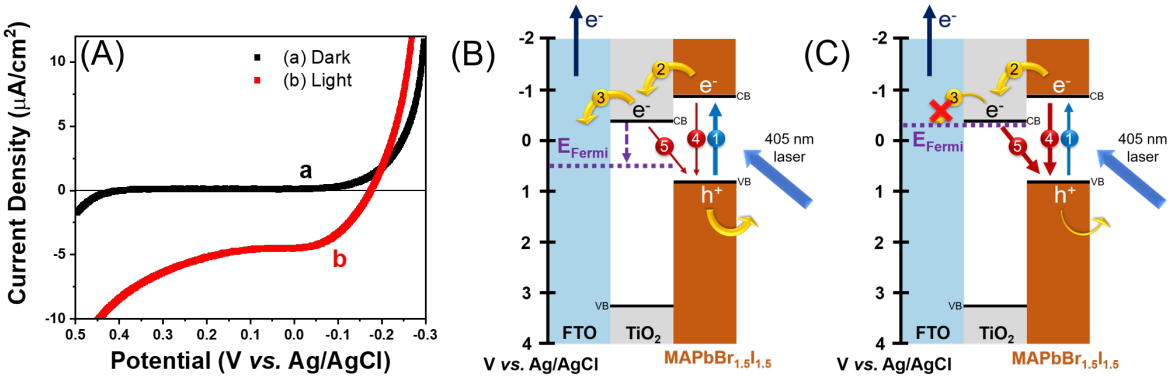

Figure 4: (A) J-V curves for $MAPbBr_{1.5}I_{1.5}$ films on FTO/TiO_2 electrode in (a) dark and (b) 405 nm CW irradiation (50 mW/cm^2). Measurements were performed in 0.01 M Bu_4NPF_6 in DCM, under degassed (N_2 saturated) conditions. (B) and (C) Band diagram scheme depicting the pathways for charge carriers when FTO/TiO_2/$MAPbBr_{1.5}I_{1.5}$ films are photoirradiated and held at (B) positive bias (+0.5 V) and (C) negative bias (-0.3 V) (*vs.* Ag/AgCl). The shifting of the Fermi level (E_{Fermi}) of the electrode and its effect on electron pathways is explicitly shown. Conduction and valence band energy levels of semiconductors are obtained from previous work (references 1 and 10).

the E_{Fermi} favors electron flow from MHP to TiO_2 and from TiO_2 to FTO (Pathways 2 and 3, Figure 4B). The accumulated holes in $MAPbBr_{1.5}I_{1.5}$ get trapped at the iodide site, which introduces instability within the lattice.[39] Because of the larger fraction of hole accumulation at positive potentials, iodine migration followed by its expulsion occurs at a faster rate. However, when we apply a negative bias (0 to -0.3 V *vs.* Ag/AgCl), E_{Fermi} shifts towards the conduction band of TiO_2. This lowers the thermodynamic driving force for electron injection, giving rise to a greater degree of charge recombination (Pathways 4 and 5, Figure 4C). This charge recombination minimizes hole accumulation in $MAPbBr_{1.5}I_{1.5}$, and thus we see slower iodine expulsion. The hole-induced oxidation or anodic corrosion of short band gap semiconductors such as metal chalcogenides in photoelectrochemical cells have been well studied.[40-42] In such instances, the surface oxidation creates a passive layer on the surface of the semiconductor as the surface gets oxidized. In MHP films, however, the interaction with holes makes iodine migrate to the interface and get expelled into the solution. The process continues until all the iodine is expelled, leaving behind a $MAPbBr_3$ perovskite film.

Morphological Changes Associated with Iodide Expulsion. The impact on morphology of the perovskite films due to photo-induced iodide expulsion under applied bias was probed using scanning electron microscopy (SEM). Pristine MHP films (before irradiation/applied bias) show a clean surface with no noticeable pinholes or voids (Figure 5A). However, upon exposure to 405 nm irradiation for 15 minutes the films exhibit voids, the degree of which is dependent on the applied bias. At -0.3 V *vs.* Ag/AgCl, we observe only a small number of pinholes (Figure 5B). At 0 V, larger pinholes are observed, and at 0.5 V these pinholes grow into larger voids indicating a greater degree of transformation of the material (Figures 5C

and D). As seen in our previous electrochemical[51] and photochemical studies[18], the perovskite structure is reconfigured following iodide expulsion, leading to poor film morphology.

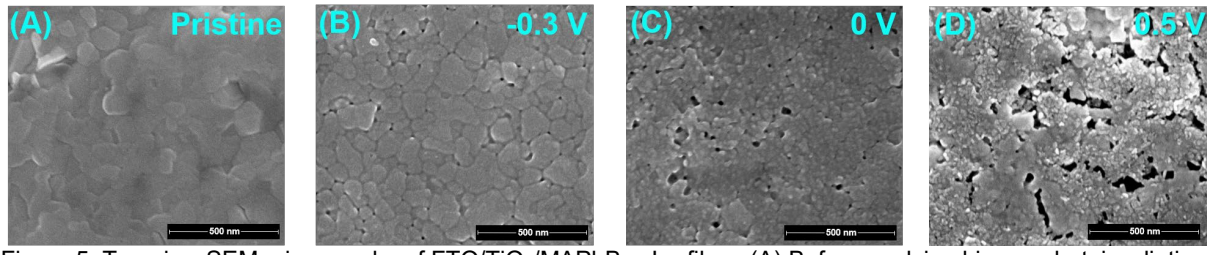

Figure 5: Top-view SEM micrographs of FTO/TiO_2/$MAPbBr_{1.5}I_{1.5}$ films. (A) Before applying bias or photoirradiation (pristine). (B-D) Films irradiated for 15 minutes with 405 nm CW laser while held at (B) -0.3 V, (C) 0 V, and (D) 0.5 V *vs.* Ag/AgCl. The void spaces which start to appear at 0 V increase in size at 0.5 V applied bias. These morphological changes seen in (C) and (D) are the result of iodine expulsion.

We also performed XPS measurements on the perovskite films to assess the change in composition that occurred during iodine expulsion. The XPS spectra are shown in Figure S13 and the results summarized in Table S3 for films held at 0.5, 0, and -0.3 V *vs.* Ag/AgCl. The film held at 0.5 V applied bias showed a large enhancement in bromine due to the greater degree of iodide removal from the film. When E_{Fermi} is shifted higher (0 V *vs.* Ag/AgCl), the films still expel iodine and become bromine-rich, but to a much smaller degree. When E_{Fermi} is shifted to the highest value (-0.3 V *vs.* Ag/AgCl), the Br/I ratio remains mostly the same, in line with the small amount of iodine expulsion.

Various models have been proposed to explain photoinduced ionic conductivity and halide migration. These include: miscibility gap between dark and illuminated conditions,[43] polaron formation and associated lattice strain,[13,44-46] trapped carrier gradient as a result of inhomogeneous excitation and defect assisted migration,[47] and positive free energies of mixing under illumination.[12,33] In a photosegregated MHP film, isoenergetic conduction band positions for $MAPb(Br_xI_{1-x})_3$, $MAPbI_3$, and $MAPbBr_3$ and valence band offsets up to 0.26-0.67 eV favor hole localization or trapping in I-rich regions.[48-50] The time scale with which various processes contributing to halide migration vary. Whereas the funneling of charge carriers to the I-rich region has been confirmed spectroscopically to occur in the time frame of 10-100 ps,[51,52] the halide segregation occurs over a period of several seconds-minutes. The ultimate expulsion of iodine occurs on a much longer time scale (in minutes–hours). Such slower expulsion of iodine has also been observed in films in contact with toluene.[17] The macroscale iodine expulsion probed in the present study further serves as a rapid test to evaluate perovskite instability caused by iodide migration. Trapping of holes at iodide sites during photoirradiation causes iodide ions to migrate toward grain boundaries, thus inducing the formation of iodide rich phases and bromide rich phases in dry films. [44,53-56] When mixed halide perovskite films are in contact with solution, however, the migration of iodine extends beyond phase segregation as it gets expelled into solution. The electrochemical modulation of iodine expulsion presented in this study further confirm the

necessity of hole localization at the iodine site as the primary step responsible for the migration if iodine in the film.

Acknowledgements

The authors thank Dr. Ian Lightcap of the Notre Dame Materials Characterization Facility (MCF) for help with and discussions about XPS, along with the Notre Dame Integrated Imaging Facility (NDIIF) for use of the SEM. J.T.D. and P.S.M. thank Gergely Samu for helpful discussions regarding electrochemical experiments. J.T.D. acknowledges support from the Patrick and Jana Eilers Graduate Student Fellowship. J.T.D. and P.V.K. acknowledge support by the Division of Chemical Sciences, Geosciences, and Biosciences, Office of Basic Energy Sciences of the U.S. Department of Energy (award DE-FC02-04ER15533) for conducting spectroelectrochemical measurements and discussions. P.S.M. and M. K. acknowledge the Division of Materials Sciences and Engineering Office of Basic Energy Sciences of the U.S. Department of Energy through Award DE-SC0014334 for carrying out iodide expulsion experiments, analysis of the data and discussions. This is contribution number NDRL No. 5297 from the Notre Dame Radiation Laboratory.

Supporting Information

Materials; preparation methods for FTO/TiO_2/perovskite electrodes; electrochemical measurements; iodide expulsion measurements; XPS data and analysis; details of SEM measurement; quantum efficiency calculation; threshold intensity (I_{th}) calculation; film stability tests; individual absorbance spectra

References

(1) Hoke, E. T.; Slotcavage, D. J.; Dohner, E. R.; Bowring, A. R.; Karunadasa, H. I.; McGehee, M. D. Reversible Photoinduced Trap Formation in Mixed-Halide Hybrid Perovskites for Photovoltaics, *Chem. Sci.* **2015,** *6*, 613-617.
(2) Brennan, M. C.; Draguta, S.; Kamat, P. V.; Kuno, M. Light-Induced Anion Phase Segregation in Mixed Halide Perovskites, *ACS Energy Lett.* **2018,** *3*, 204-213.
(3) Li, W., et al. Phase Segregation Enhanced Ion Movement in Efficient Inorganic $CsPbIBr_2$ Solar Cells, *Adv. Energy Mater.* **2017,** *7*, Article Number: 1700946.
(4) DuBose, J. T.; Kamat, P. V. TiO_2-Assisted Halide Ion Segregation in Mixed Halide Perovskite Films, *J. Am. Chem. Soc.* **2020,** *142*, 5362-5370.
(5) Brennan, M. C.; Ruth, A.; Kamat, P. V.; Kuno, M. Photoinduced Anion Segregation in Mixed Halide Perovskites, *Trends in Chemistry* **2020,** *2*, 282-301.
(6) Vicente, J. R.; Chen, J. Phase Segregation and Photothermal Remixing of Mixed-Halide Lead Perovskites, *J. Phys. Chem. Lett.* **2020,** *11*, 1802-1807.
(7) Samu, G. F.; Janáky, C.; Kamat, P. V. A Victim of Halide Ion Segregation. How Light Soaking Affects Solar Cell Performance of Mixed Halide Lead Perovskites, *ACS Energy Lett.* **2017,** *2*, 1860-1861.
(8) Balakrishna, R. G.; Kobosko, S. M.; Kamat, P. V. Mixed Halide Perovskite Solar Cells. Consequence of Iodide Treatment on Phase Segregation Recovery, *ACS Energy Lett.* **2018,** *3*, 2267-2272.
(9) Vashishtha, P.; Halpert, J. E. Field-Driven Ion Migration and Color Instability in Red-Emitting Mixed Halide Perovskite Nanocrystal Light-Emitting Diodes, *Chem. Mater.* **2017,** *29*, 5965-5973.

(10) Elmelund, T.; Scheidt, R. A.; Seger, B.; Kamat, P. V. Bidirectional Halide Ion Exchange in Paired Lead Halide Perovskite Films with Thermal Activation, *ACS Energy Lett.* **2019,** *4*, 1961-1969.
(11) Ruth, A.; Brennan, M. C.; Draguta, S.; Morozov, Y. V.; Zhukovskyi, M.; Janko, B.; Zapol, P.; Kuno, M. Vacancy-Mediated Anion Photosegregation Kinetics in Mixed Halide Hybrid Perovskites: Coupled Kinetic Monte Carlo and Optical Measurements, *ACS Energy Lett.* **2018,** *3*, 2321-2328.
(12) Elmelund, T.; Seger, B.; Kuno, M.; Kamat, P. V. How Interplay between Photo and Thermal Activation Dictates Halide Ion Segregation in Mixed Halide Perovskites, *ACS Energy Lett.* **2020,** *5*, 56-63.
(13) Muscarella, L. A., et al. Lattice Compression Increases the Activation Barrier for Phase Segregation in Mixed-Halide Perovskites, *ACS Energy Lett.* **2020**, 3152-3158.
(14) Belisle, R. A.; Bush, K. A.; Bertoluzzi, L.; Gold-Parker, A.; Toney, M. F.; McGehee, M. D. Impact of Surfaces on Photoinduced Halide Segregation in Mixed-Halide Perovskites, *ACS Energy Lett.* **2018,** *3*, 2694-2700.
(15) Cho, J.; Kamat, P. V. How Chloride Suppresses Photoinduced Phase Segregation in Mixed Halide Perovskites, *Chem. Mater.* **2020,** *32*, 6206–6212.
(16) Cho, J.; DuBose, J. T.; Le, A. N. T.; Kamat, P. V. Suppressed Halide Ion Migration in 2D Lead Halide Perovskites, *ACS Materials Lett.* **2020,** *2*, 565-570.
(17) Kim, G. Y.; Senocrate, A.; Yang, T.-Y.; Gregori, G.; Grätzel, M.; Maier, J. Large Tunable Photoeffect on Ion Conduction in Halide Perovskites and Implications for Photodecomposition, *Nature Mater.* **2018,** *17*, 445-449.
(18) Mathew, P. S.; Samu, G. F.; Janáky, C.; Kamat, P. V. Iodine (I) Expulsion at Photoirradiated Mixed Halide Perovskite Interface. Should I Stay or Should I Go?, *ACS Energy Lett.* **2020,** *5*, 1872-1880.
(19) Brennan, M. C.; Toso, S.; Pavlovetc, I. M.; Zhukovskyi, M.; Marras, S.; Kuno, M.; Manna, L.; Baranov, D. Superlattices are Greener on the Other Side: How Light Transforms Self-Assembled Mixed Halide Perovskite Nanocrystals, *ACS Energy Lett.* **2020,** *5*, 1465-1473.
(20) Wang, S. H.; Jiang, Y.; Juarez-Perez, E. J.; Ono, L. K.; Qi, Y. B. Accelerated Degradation of Methylammonium Lead Iodide Perovskites Induced by Exposure to Iodine Vapour, *Nature Energy* **2017,** *2*, Art. No. 16195.
(21) Sutter-Fella, C. M., et al. Cation-Dependent Light-Induced Halide Demixing in Hybrid Organic–Inorganic Perovskites, *Nano Lett.* **2018,** *18*, 3473-3480.
(22) Ferdani, D. W., et al. Partial Cation Substitution Reduces Iodide Ion Transport in Lead Iodide Perovskite Solar Cells, *Energy & Environ. Sci.* **2019,** *12*, 2264-2272.
(23) Xu, J., et al. Triple-Halide Wide–Band Gap Perovskites with Suppressed Phase Segregation for Efficient Tandems, *Science* **2020,** *367*, 1097-1104.
(24) Ma, D. X., et al. Chloride Insertion-Immobilization Enables Bright, Narrowband, and Stable Blue-Emitting Perovskite Diodes, *J. Am. Chem. Soc.* **2020,** *142*, 5126-5134.
(25) Xiao, Z., et al. Mixed-Halide Perovskites with Stabilized Bandgaps, *Nano Lett.* **2017,** *17*, 6863-6869.
(26) Huang, Z., et al. Suppressed Ion Migration in Reduced-Dimensional Perovskites Improves Operating Stability, *ACS Energy Lett.* **2019**, 1521-1527.
(27) Lin, Y.-H., et al. A Piperidinium Salt Stabilizes Efficient Metal-Halide Perovskite Solar Cells, *Science* **2020,** *369*, 96-102.
(28) Ravi, V. K.; Markad, G. B.; Nag, A. Band Edge Energies and Excitonic Transition Probabilities of Colloidal $CsPbX_3$ (X = Cl, Br, I) Perovskite Nanocrystals, *ACS Energy Lett.* **2016,** *1*, 665-671.
(29) Shallcross, R. C.; Zheng, Y.; Saavedra, S. S.; Armstrong, N. R. Determining Band-Edge Energies and Morphology-Dependent Stability of Formamidinium Lead Perovskite Films Using Spectroelectrochemistry and Photoelectron Spectroscopy, *J. Am. Chem. Soc.* **2017,** *139*, 4866-4878.
(30) Lorenzon, M., et al. Role of Nonradiative Defects and Environmental Oxygen on Exciton Recombination Processes in $CsPbBr_3$ Perovskite Nanocrystals, *Nano Lett.* **2017,** *17*, 3844-3853.

(31) Samu, G. F.; Scheidt, R. A.; Kamat, P. V.; Janáky, C. Electrochemistry and Spectroelectrochemistry of Lead Halide Perovskite Films: Materials Science Aspects and Boundary Conditions, *Chem. Mater.* **2018,** *30*, 561-569.
(32) Samu, G. F.; Balog, Á.; De Angelis, F.; Meggiolaro, D.; Kamat, P. V.; Janáky, C. Electrochemical Hole Injection Selectively Expels Iodide from Mixed Halide Perovskite Films, *J. Am. Chem. Soc.* **2019,** *141*, 10812-10820.
(33) Draguta, S.; Sharia, O.; Yoon, S. J.; Brennan, M. C.; Morozov, Y. V.; Manser, J. M.; Kamat, P. V.; Schneider, W. F.; Kuno, M. Rationalizing the Light-Induced Phase Separation of Mixed Halide Organic-Inorganic Perovskites, *Nature Commun.* **2018,** *8*, Article No. 200 (DOI: 10.1038/s41467-017-00284-2).
(34) Kojima, A.; Teshima, K.; Shirai, Y.; Miyasaka, T. Organometal Halide Perovskites as Visible-Light Sensitizers for Photovoltaic Cells, *J. Am. Chem. Soc.* **2009,** *131*, 6050-6051.
(35) Im, J.-H.; Lee, C.-R.; Lee, J.-W.; Park, S.-W.; Park, N.-G. 6.5%Efficient Perovskite Quantum-Dot-Sensitized Solar Cell. Nanoscale, *Nanoscale* **2011**, 4088−4093.
(36) Hsu, H.-Y.; Ji, L.; Ahn, H. S.; Zhao, J.; Yu, E. T.; Bard, A. J. A Liquid Junction Photoelectrochemical Solar Cell Based on p-Type $MeNH_3PbI_3$ Perovskite with 1.05 V Open-Circuit Photovoltage, *J. Am. Chem. Soc.* **2015,** *137*, 14758-14764.
(37) Scheidt, R. A.; Samu, G. F.; Janáky, C.; Kamat, P. V. Modulation of Charge Recombination in $CsPbBr_3$ Perovskite Films with Electrochemical Bias, *J. Am. Chem. Soc.* **2018,** *140*, 86-89.
(38) Scheidt, R. A.; Kerns, E.; Kamat, P. V. Interfacial Charge Transfer between Excited $CsPbBr_3$ Nanocrystals and TiO_2: Charge Injection versus Photodegradation, *J. Phys. Chem. Lett.* **2018,** *9*, 5962-5969.
(39) Motti, S. G., et al. Controlling Competing Photochemical Reactions Stabilizes Perovskite Solar Cells, *Nature Photonics* **2019,** *13*, doi: 10.1038/s41566-019-0435-1.
(40) Ellis, A. B.; Kaiser, S. W.; Bolts, J. M.; Wrighton, M. S. Study of n-type Semiconducting Cadmium Chalcogenide- Based Photoelectrochemical Cells Employing Polychalcogenide Electrolytes, *J. Am. Chem. Soc.* **1977,** *99*, 2839-2848.
(41) Tenne, R. Performance and Stability of CdSe/Polysulfide Photoelectrochemical Cells Under Chopped Illumination, *J. Electroanal. Chem. Interfacial Electrochem* **1983,** *143*, 113-20.
(42) Bang, J. H.; Kamat, P. V. Quantum Dot Sensitized Solar Cells. A Tale of Two Semiconductor Nanocrystals: CdSe and CdTe, *ACS Nano* **2009,** *3*, 1467-1476.
(43) Brivio, F.; Caetano, C.; Walsh, A. Thermodynamic Origin of Photoinstability in the $CH_3NH_3Pb(I_{1-x}Br_x)_3$ Hybrid Halide Perovskite Alloy, *J. Phys. Chem. Lett.* **2016,** *7*, 1083-1087.
(44) Bischak, C. G.; Hetherington, C. L.; Wu, H.; Aloni, S.; Ogletree, D. F.; Limmer, D. T.; Ginsberg, N. S. Origin of Reversible Photoinduced Phase Separation in Hybrid Perovskites, *Nano Lett.* **2017,** *17*, 1028-1033.
(45) Bischak, C. G.; Wong, A. B.; Lin, E.; Limmer, D. T.; Yang, P.; Ginsberg, N. S. Tunable Polaron Distortions Control the Extent of Halide Demixing in Lead Halide Perovskites, *J. Phys. Chem. Lett.* **2018,** *9*, 3998-4005.
(46) Wang, X., et al. Suppressed Phase Separation of Mixed-Halide Perovskites Confined in Endotaxial Matrices, *Nature Commun.* **2019,** *10*, 695.
(47) Barker, A. J., et al. Defect-Assisted Photoinduced Halide Segregation in Mixed-Halide Perovskite Thin Films, *ACS Energy Lett.* **2017,** *2*, 1416–1424.
(48) Schulz, P.; Edri, E.; Kirmayer, S.; Hodes, G.; Cahen, D.; Kahn, A. Interface Energetics in Organo-Metal Halide Perovskite-Based Photovoltaic Cells, *Energy & Environ. Sci.* **2014,** *7*, 1377-1381.
(49) Butler, K. T.; Frost, J. M.; Walsh, A. Band Alignment of the Hybrid Halide Perovskites $CH_3NH_3PbCl_3$, $CH_3NH_3PbBr_3$ and $CH_3NH_3PbI_3$, *Materials Horizons* **2015,** *2*, 228-231.

(50) Yoon, S. J.; Draguta, S.; Manser, J. S.; Sharia, O.; Schneider, W. F.; Kuno, M.; Kamat, P. V. Tracking Iodide and Bromide Ion Segregation in Mixed Halide Lead Perovskites during Photoirradiation, *ACS Energy Lett.* **2016,** *1*, 290-296.
(51) Hoffman, J. B.; Schleper, A. L.; Kamat, P. V. Transformation of Sintered $CsPbBr_3$ Nanocrystals to Cubic $CsPbI_3$ and Gradient $CsPbBr_xI_{3-x}$ through Halide Exchange, *J. Am. Chem. Soc.* **2016,** *138*, 8603–8611.
(52) Scheidt, R. A.; Kamat, P. V. Temperature-Driven Anion Migration in Gradient Halide Perovskites, *J. Chem. Phys.* **2019,** *151*, Art. No. 134703.
(53) Li, W., et al. Phase Segregation Enhanced Ion Movement in Efficient Inorganic CsPbIBr2 Solar Cells, *Advanced Energy Materials* **2017,** *7*, 1700946.
(54) Rehman, W.; McMeekin, D. P.; Patel, J. B.; Milot, R. L.; Johnston, M. B.; Snaith, H. J.; Herz, L. M. Photovoltaic Mixed-Cation Lead Mixed-Halide Perovskites: Links between Crystallinity, Photostability and Electronic Properties, *Energy & Environ. Sci.* **2017,** *10*, 361-369.
(55) Tang, X.; van den Berg, M.; Gu, E.; Horneber, A.; Matt, G. J.; Osvet, A.; Meixner, A. J.; Zhang, D.; Brabec, C. J. Local Observation of Phase Segregation in Mixed-Halide Perovskite, *Nano Lett.* **2018,** *18*, 2172-2178.
(56) Knight, A. J.; Patel, J. B.; Snaith, H. J.; Johnston, M. B.; Herz, L. M. Trap States, Electric Fields, and Phase Segregation in Mixed-Halide Perovskite Photovoltaic Devices, *Adv. Energy Mater.* **2020,** *10*, 1903488.

Supporting Information

Modulation of Photo Induced Iodine Expulsion in Mixed Halide Perovskites with Electrochemical Bias

Jeffrey T. DuBose[1,2,#] Preethi S. Mathew[1,2,#] Junsang Cho[1], Masaru Kuno[2] and Prashant V. Kamat[1,2,3*]

[1]Notre Dame Radiation Laboratory, [2]Department of Chemistry and Biochemistry, and [3]Department of Chemical and Biomolecular Engineering.
University of Notre Dame, Notre Dame, Indiana 46556, United States

---

# Equal contribution

* Address correspondence to this author pkamat@nd.edu

1. Materials / Methods

Materials: Methylammonium iodide (MAI; Greatcell Solar), methylammonium bromide (MABr; Greatcell Solar), Lead iodide (PbI_2, ultra-dry, 10 mesh beads, 99.999% metals basis, Alfa Aesar), Lead bromide ($PbBr_2$, Alfa Aesar. 99.999%), dimethyl sulfoxide (DMSO, anhydrous, ≥99.9%, Sigma-Aldrich), diethyl ether (inhibitor-free, ≥99.9%, Sigma-Aldrich), TiO_2 paste (30 NR-D, ~30 nm particle size, Greatcell Solar), N,N-dimethylformamide (anhydrous, 99.8%, Sigma-Aldrich), dichloromethane (DCM, anhydrous, ≥99.8%, contains 40-150 ppm amylene as stabilizer, Sigma-Aldirch), tetrabutylammonium hexafluorophosphate (Bu_4NPF_6, Sigma-Aldrich), were all used directly from the supplier without further purification.

FTO/TiO_2 film preparation: Films were prepared on 2.5 cm x 2.5 cm fluorine-doped tin oxide (FTO) substrates (TEC7, ~7Ω/sq sheet resistance, Greatcell). 0.416g TiO_2 paste was added to 3.5 mL ethanol and the solution was vortex mixed until homogenous and then sonicated for 15 min. 250 μL of the diluted TiO_2 paste was spin coated onto FTO at 2000 rpm for 20 sec (with acceleration time of 1.6 sec and deceleration time of 2.0 sec). The films were annealed at 550 °C for 1 hr in air.

$MAPbBr_{1.5}I_{1.5}$ Film Deposition: Each of the following steps were carried out in a glovebox to minimize exposure to air/water. 0.3 M PbI_2, 0.3 M $PbBr_2$, 0.3 M MAI and 0.3 M MABr were dissolved in DMF along with DMSO (0.6 M) and stirred for 1 hr. The solution was then filtered through a 0.1 μm PTFE filter. Then 50 μL of the solution was added statically added to the previously made FTO/TiO_2 substrates, then immediately spun at 4000 rpm for 25 sec (acceleration of 1200 rpm). Exactly 10 sec after start, 0.5 mL of diethyl ether was added as the anti-solvent. After spin-coating, the film was heated at 65 °C for 1 min on a hot plate, then transferred to another hot plate to anneal for 2 min at 100 °C. To homogenize the composition, the films were annealed at 65 °C overnight (protected by glass slide encapsulation to prevent evaporation of methylammonium). After cooling to room temperature, the films were stored in the glovebox until measurements were made.

Electrochemical Measurements: Measurements were carried out with a Gamry potentiostat in a standard three-electrode setup. The FTO/TiO_2/ $MAPbBr_{1.5}I_{1.5}$ acted as the working electrode, a Pt mesh was the counter electrode and an Ag/AgCl wire was the pseudoreference electrode. Measurements were performed under inert atmosphere (N_2 pre-bubbled through DCM to reduce DCM evaporation in the cell), and the electrolyte used was 0.01 M Bu_4NPF_6 in DCM.

The pseudoreference electrode was calibrated by measuring the formal potential of the ferrocene/ferrocenium redox couple in DCM. The formal potential was found to be E = 330 mV vs. our Ag/AgCl ($E_{Fc/Fc+}$ = 440 mV) by analysis of cyclic voltammograms at several sweep rates, in line with previous results[1-3].

Steady State Absorbance and Spectroelectrochemical Measurements: Steady state absorbance spectra were obtained from a Cary 50 Bio spectrophotometer (Varian). Spectroelectrochemical measurements were performed using the above-mentioned parameters.

Iodide Expulsion: Iodide expulsion was induced by photoirradiating the FTO/TiO_2/$MAPbBr_{1.5}I_{1.5}$ films with a 405 nm continuous (CW) laser (50 mW/cm^2) while the films were held at various applied potentials. Absorbance spectra of the films were recorded over time to monitor the expulsion process. All measurements were done under inert atmosphere (N_2 pre-bubbled through DCM to reduce DCM evaporation in the cell), and the electrolyte used was 0.01 M Bu_4NPF_6 in DCM. A 428 nm longpass filter was placed in front of the UV-vis spectrophotometer to cut out any scatter from the 405 nm laser.

XPS Measurements: The surface characterization of the films was performed using X-ray Photolectron Spectroscopy (XPS) on a PHI VersaProbe II. Spectra were calibrated against the C1s peak @ 285.3 eV[4].

SEM Measurements: Top-down Scanning Electron Microscopy (SEM) images were taken using a FEI SEM Magellan 400 digital field emission microscope with a beam voltage of 2 kV.

1a. Quantum Efficiency (QE) of Iodide Expulsion:

From the absorbance (Figure 2, main text) and film morphology measurements (SEM: Figure 5 main text; XPS: Figure S13 & Table S3) a clear loss of iodide is observed in the perovskite films when subjected to irradiation. The question that arises is where does this iodide go? In our previous study[3] we found that dissolution of primarily iodide species occurs from films subjected to electrochemical hole injection. Additionally, in our previous photochemical study of Cs-alloyed $MAPbBr_{1.5}I_{1.5}$ films under photoirradiation, we were able to track the expulsion of iodide by monitoring the UV-vis absorbance of I_3^- in solution[5].

Potential (V vs. Ag/AgCl)	Quantum Efficiency (%)
0.5	4.2×10^{-2}
0	1.5×10^{-2}
-0.3	0.44×10^{-2}

Table S1: Quantum efficiency (QE) values for iodide expulsion, calculated from the I_3^- absorbance.

We measured the absorbance spectrum of our solution as we carried out iodide expulsion. FTO/TiO_2/$MAPbBr_{1.5}I_{1.5}$ films were held at 0.5, 0, and -0.3 V vs. Ag/AgCl and irradiated for 15 minutes (405 nm, 50 mW/cm^2) The absorbance of the solution after 15 minutes of irradiation shows characteristic absorbance peaks at 298 and 364 nm of I_3^- species (Figure S5), which confirms the presence of this predominant species[6]. We calculated the quantum efficiency (QE) of iodide expulsion using the equation S1:

$$QE(\%) = 100 \times \frac{3n_{I_3^-}}{2n_{photons}} \qquad \textbf{(eq S1)}$$

where $n_{I_3^-}$ is the moles of I_3^- produced and $n_{photons}$ is the number of photons hitting the sample. For the formation of one I_3^- species, three I species are expelled induced by two photons (see below). The quantum efficiency values at different potentials are summarized in Table S1. We find that after irradiating for the same time (15 minutes) at different potentials, the film held at 0.5 V vs. Ag/AgCl had the highest quantum efficiency of iodide expulsion (4.2×10^{-2} %). When held at -0.3 V vs. Ag/AgCl, the E_{Fermi} is raised such that iodide expulsion is less favorable, and we see an order of magnitude lower QE of 0.44×10^{-2} %. These results further establish the influence of applied bias on the iodide expulsion process.

Derivation of QE expression:

From the absorbance spectrum of the electrolyte solution, the concentration of the triiodide species was calculated by Beer's Law. The absorption coefficient of triiodide at 364 nm (2.32×10^4 L/mol)[3,6] was used to calculate the concentration of triiodide expelled from the film held at different potentials for the same amount of time. The number of photons, $n_{photons}$ corresponding to the energy of photons emitted by the lamp is given by equation S2:

$$n_{photons} = (\text{Power}/E)/N_A \qquad \textbf{(eq S2)}$$

where E is the energy of the 405 nm laser and N_A is the Avogadro's constant. We calculated the number of photons absorbed by the perovskite in 15 min to be 116 mmol. The quantum efficiency of this process for iodide expulsion was determined from the ratio of the number of 3/2(moles triiodide species ($n_{I_3^-}$) and

$n_{photons}$ (equation S1). Since one mole of I_3^- corresponds to 3 iodide species following the absorption of 2 photons[3,5], we employed a multiplication factor of 3/2.

1b. Threshold Intensity Determination:

To determine a threshold intensity ($I_{Threshold}$) to induce iodide expulsion in the FTO/TiO_2/$MAPbBr_{1.5}I_{1.5}$ films held at several applied potentials, we performed our standard iodide expulsion experiment (details found in Section 1 of the SI) at low excitation intensities ($\mu W/cm^2$ range). As before, we used 0.01 M Bu_4NPF_6 in DCM as the electrolyte, ran the experiment under N_2 (which was pre-bubbled through DCM to reduce solvent loss), and photoirradiated with a 405 nm CW laser for 60 minutes.

From the dark stability experiments (Figures S3 & S4) we could see that even without irradiation, a small blueshift of the band edge absorbance occurs (typically in the range of 3-6 nm). This is likely due to a small amount of dissolution due to the presence of electrolyte[2,3]. Thus, to distinguish between the small band edge shift due to electrolyte contact and the shift in the band edge due to iodide expulsion, we decided to use a band edge shift that was twice the shift in the dark to be indicative of light-induced iodide expulsion. In other words, if the band edge shift in the dark was X (in nm), we used a shift of ~2X as our basis for what constituted iodide expulsion.

Figure S11 shows the absorption spectra of the films used to determine the threshold intensity for iodide expulsion at the 3 potentials used. Table S2 summarizes the results for films held at 0.5, 0, and -0.3 V vs. Ag/AgCl, and Figure S12 graphically depicts the results. Due to fluctuations in laser intensity, we could not accurately adjust the intensity in the low $\mu W/cm^2$ range (i.e. we could not reliably confirm the intensity to be precisely 100 vs. 120 $\mu W/cm^2$), so for the perovskite films held at 0.5 and -0.3 V vs. Ag/AgCl we linearly interpolated between the data for two intensities to estimate the intensity that corresponded to a 2X shift. This uncertainty is reflected in the error bars given in Figure S12.

Potential (V vs. Ag/AgCl)	Light Intensity	Band EdgeShift (nm)	$Shift_{light}/Shift_{dark}$	Linearly Interpolated Threshold Intensity ($I_{Threshold}$, $\mu W/cm^2$)
0.5 V	Dark	3.1	--	66
	65 $\mu W/cm^2$	5.0	1.6	
	130 $\mu W/cm^2$	57.0	18.5	
0 V	Dark	2.9	--	--
	260 $\mu W/cm^2$	6.0	2.1	
-0.3 V	Dark	6.0	--	285
	260 $\mu W/cm^2$	7.9	1.3	
	315 $\mu W/cm^2$	17.0	2.8	

Table S2. Results of the threshold intensity determination. A ratio of the band edge shift under irradiation ($Shift_{light}$) divided by the band edge shift that occurs in the dark ($Shift_{dark}$) of 2 was used to define the onset of light-induced iodide expulsion.

2. Figures S1-S13; Scheme S1; Table S3

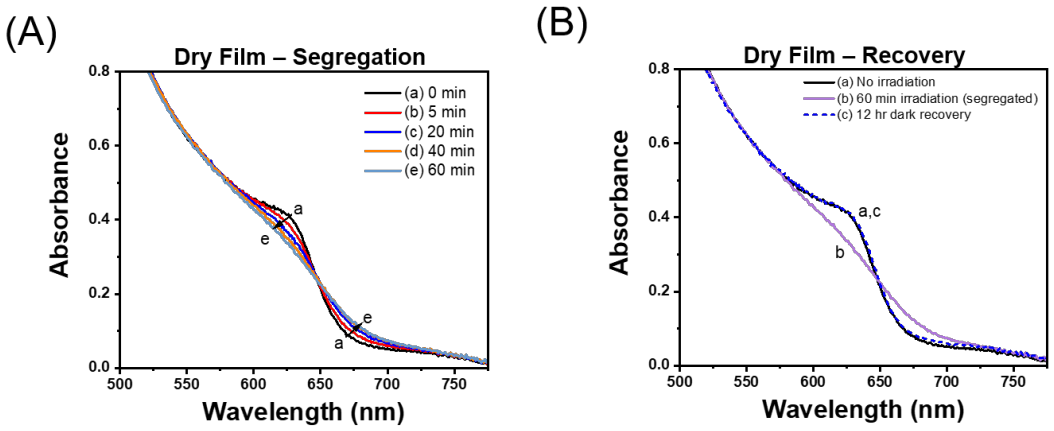

Figure S1. (A) Phase segregation of a dry $MAPbBr_{1.5}I_{1.5}$ film under 405 nm CW irradiation (50 mW/cm^2). (B) Dark recovery of the mixed $MAPbBr_{1.5}I_{1.5}$ phase after overnight (12 hr) recovery, indicating reversibility of the process.

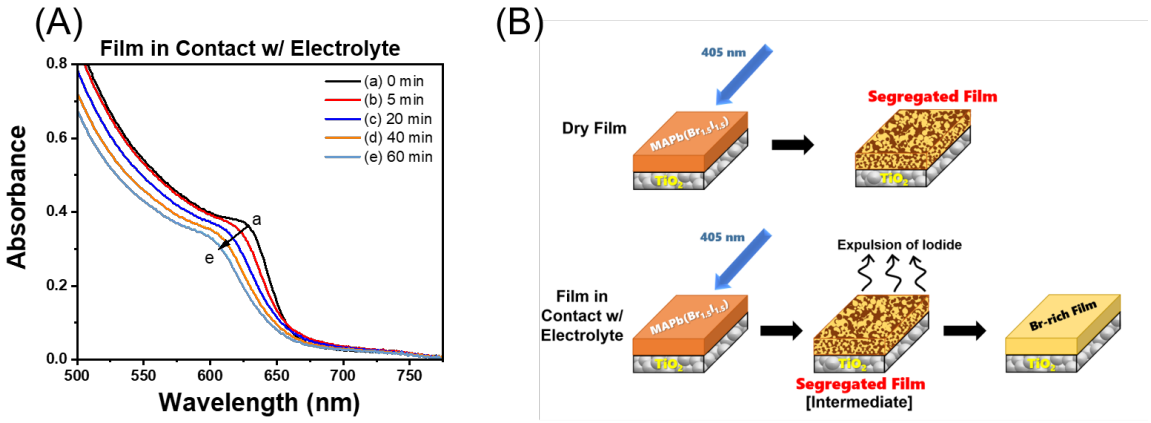

Figure S2. Absorbance spectra of $MAPbBr_{1.5}I_{1.5}$ film under 405 nm CW irradiation (A) in contact with 0.01 M Bu_4NPF_6 electrolyte in DCM. (B) Schematic representation of the processes occurring when $MAPbBr_{1.5}I_{1.5}$ films are photoirradiated in dry condition and when exposed to electrolyte. Note that the electrolyte Bu_4NPF_6 is not necessarily needed for iodide expulsion; iodide expulsion can occur in non-polar solvents like toluene[7] or DCM[5] alone.

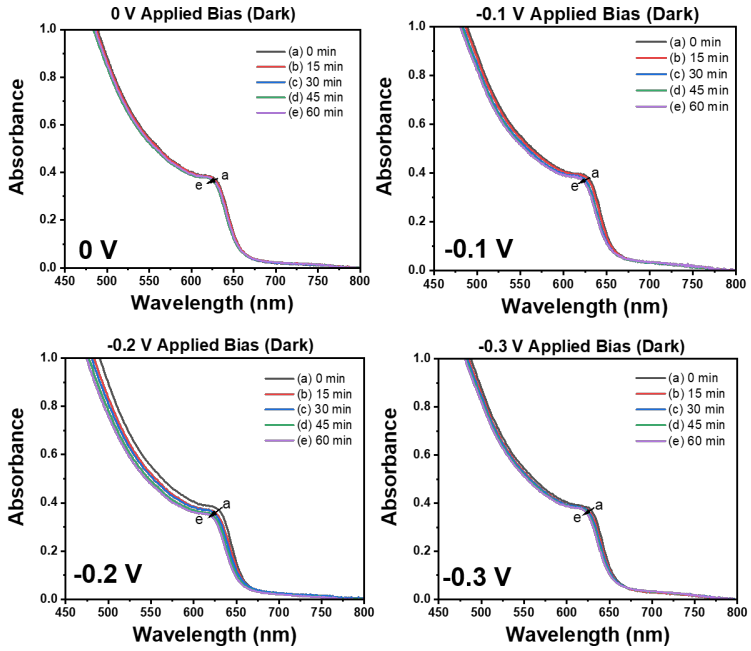

Figure S3. Stability of FTO/TiO_2/$MAPbBr_{1.5}I_{1.5}$ films held at cathodic biases of -0.1 to -0.3 V *vs.* Ag/AgCl in dark conditions for 1 hour. Measurements were performed in 0.01 M Bu_4NPF_6 in DCM, under degassed N_2 conditions (pre-bubbled through DCM).

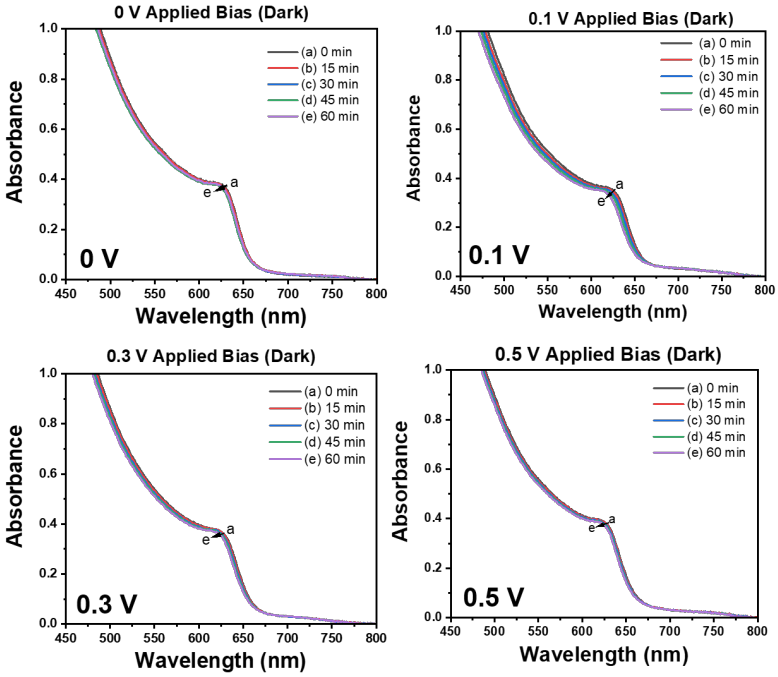

Figure S4. Stability of FTO/TiO_2/$MAPbBr_{1.5}I_{1.5}$ films held at anodic biases of 0.1 to 0.5 V *vs.* Ag/AgCl in dark conditions for 1 hour. Measurements were performed in 0.01 M Bu_4NPF_6 in DCM, under degassed N_2 conditions (pre-bubbled through DCM).

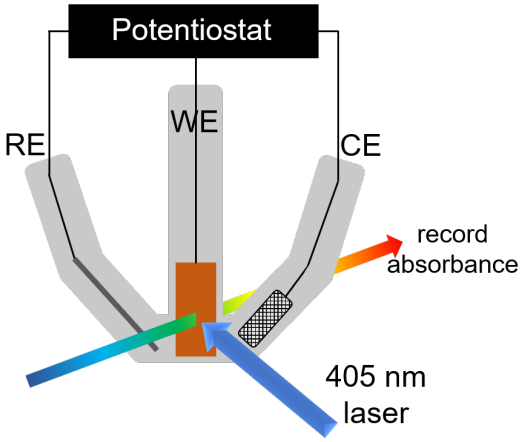

Scheme S1: Schematic representation of the experimental spectroelectrochemical set-up with 405 nm CW laser irradiation. RE = reference electrode (Ag/AgCl pseudoreference electrode), WE = working electrode (FTO/TiO_2/$MAPbBr_{1.5}I_{1.5}$), CE = counter electrode (Pt mesh).

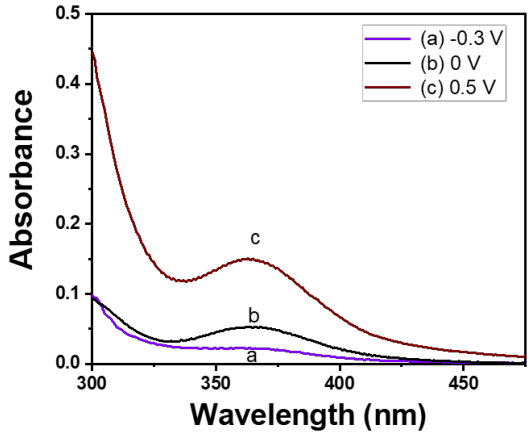

Figure S5: Absorbance spectra of the electrolyte solution after irradiating FTO/TiO_2/$MAPbBr_{1.5}I_{1.5}$ films with 405 nm CW laser for 15 min (50 mW/cm^2) at (a) -0.3 V (b) 0 V and (c) 0.5 V *vs.* Ag/AgCl. The appearance of peaks near 300 nm and 364 nm indicate formation of I_3^-.

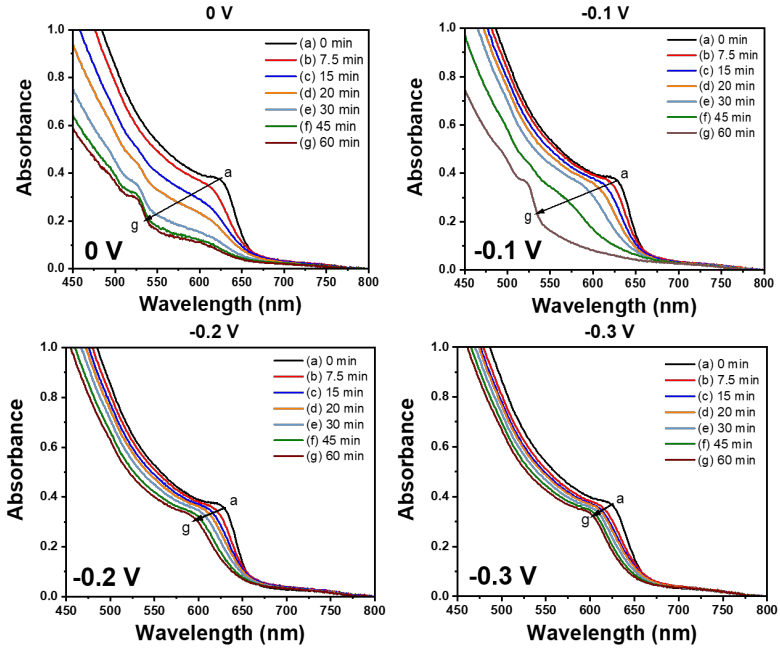

Figure S6. Iodide expulsion at cathodic bias. Absorbance spectra of FTO/TiO_2/$MAPbBr_{1.5}I_{1.5}$ films during 405 nm CW photoirradiation (50 mW/cm^2) while held at each cathodic bias (-0.1 to -0.3 V *vs.* Ag/AgCl). Measurements were performed in 0.01 M Bu_4NPF_6 in DCM, under degassed N_2 conditions (pre-bubbled through DCM).

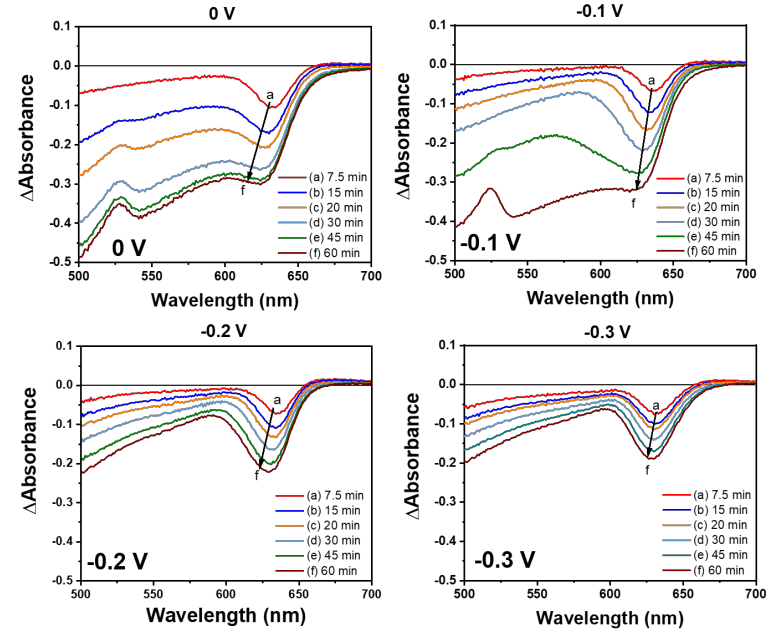

Figure S7. Iodide expulsion at cathodic bias. Corresponding ΔAbsorbance spectra of FTO/TiO_2/$MAPbBr_{1.5}I_{1.5}$ films during 405 nm CW photoirradiation (50 mW/cm^2) while held at each cathodic bias (-0.1 to -0.3 V *vs.* Ag/AgCl). Measurements were performed in 0.01 M Bu_4NPF_6 in DCM, under degassed N_2 conditions (pre-bubbled through DCM).

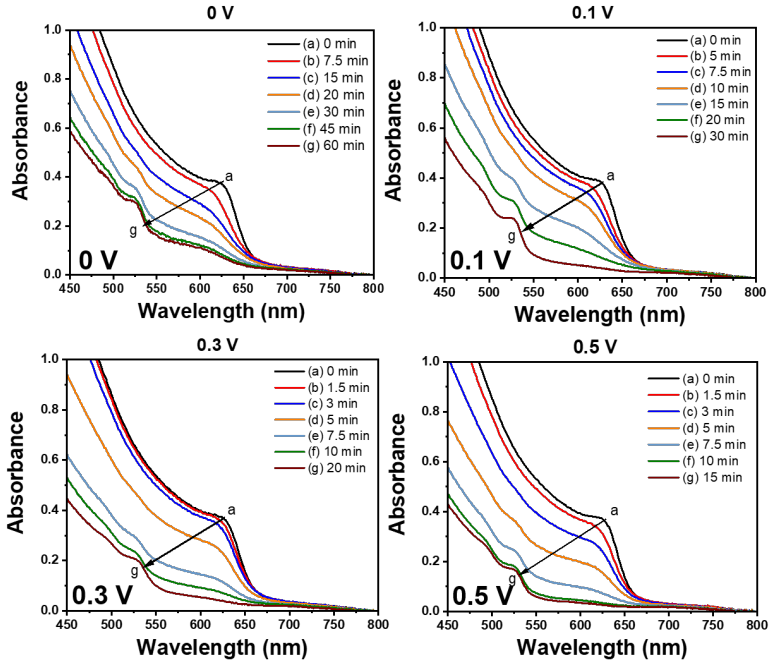

Figure S8. Iodide expulsion at anodic bias. Absorbance spectra of FTO/TiO_2/$MAPbBr_{1.5}I_{1.5}$ films during 405 nm CW photoirradiation (50 mW/cm^2) while held at each anodic bias (0.1 to 0.5 V *vs.* Ag/AgCl). Measurements were performed in 0.01 M Bu_4NPF_6 in DCM, under degassed N_2 conditions (pre-bubbled through DCM).

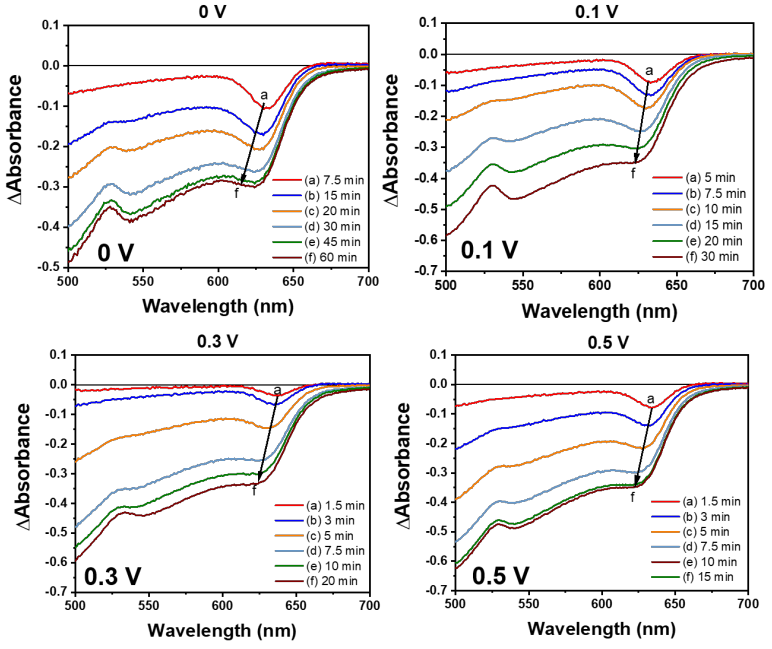

Figure S9. Iodide expulsion at anodic bias. Corresponding ΔAbsorbance spectra of FTO/TiO_2/$MAPbBr_{1.5}I_{1.5}$ films during 405 nm CW (50 mW/cm^2) photoirradiation while held at each anodic bias (0.1 to 0.5 V *vs.* Ag/AgCl). Measurements were performed in 0.01 M Bu_4NPF_6 in DCM, under degassed N_2 conditions (pre-bubbled through DCM).

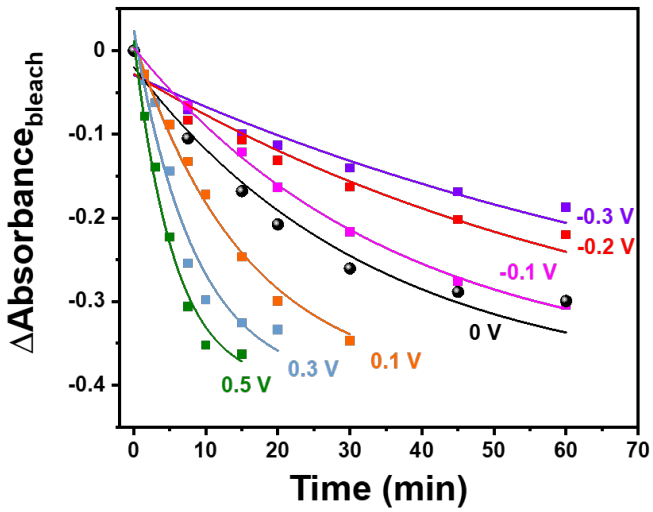

Figure S10: Monoexponential fits to the differential absorbance bleach feature for FTO/TiO_2/$MAPbBr_{1.5}I_{1.5}$ films that underwent iodide expulsion at all studied potentials ranging from 0.5 to -0.3 V *vs.* Ag/AgCl.

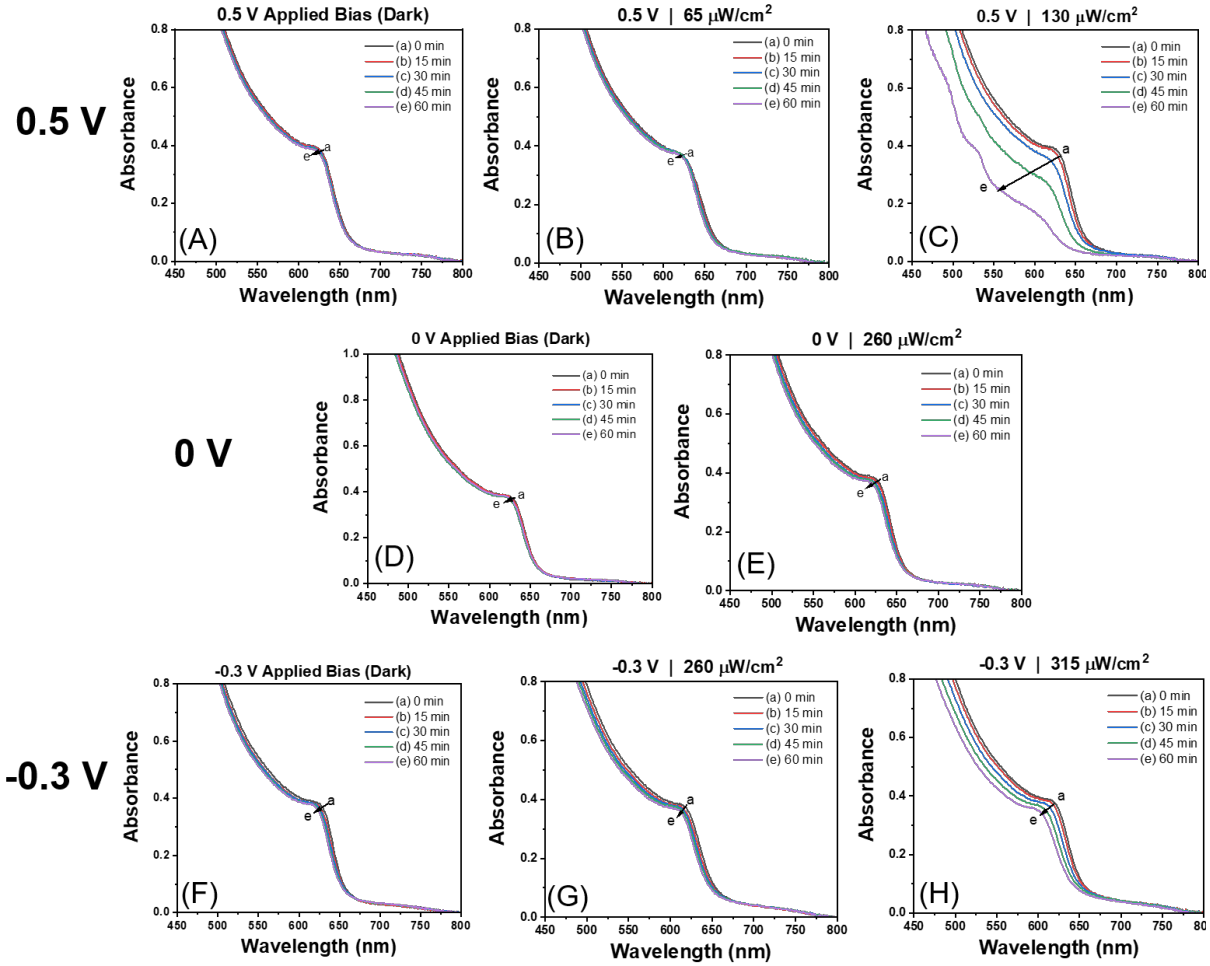

Figure S11: Absorption spectra of FTO/TiO_2/$MAPbBr_{1.5}I_{1.5}$ films used to determine threshold intensity for inducing iodide expulsion ($I_{Threshold}$). (A-C) Films held at 0.5 V *vs.* Ag/AgCl under (A) dark, (B) 65, and (C) 130 μW/cm^2 405 nm irradiation. (D-E) Films held at 0 V *vs.* Ag/AgCl under (D) dark and (E) 260 μW/cm^2 405 nm irradiation. (F-H) Films held at -0.3 V *vs.* Ag/AgCl under (F) dark, (G) 260, and (H) 315 μW/cm^2 405 nm irradiation.

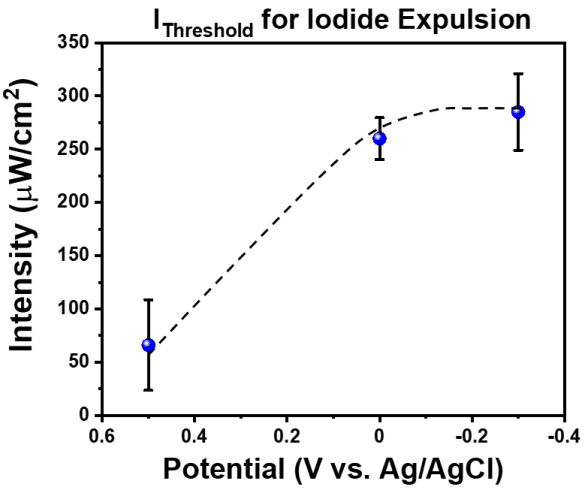

Figure S12: Threshold irradiation intensity ($I_{Threshold}$) needed to induce iodide expulsion in $MAPbBr_{1.5}I_{1.5}$ films held at various potentials. Individual absorbance spectra used to determine $I_{Threshold}$ are given in Figure S11. The dashed line acts as a guide to the eye.

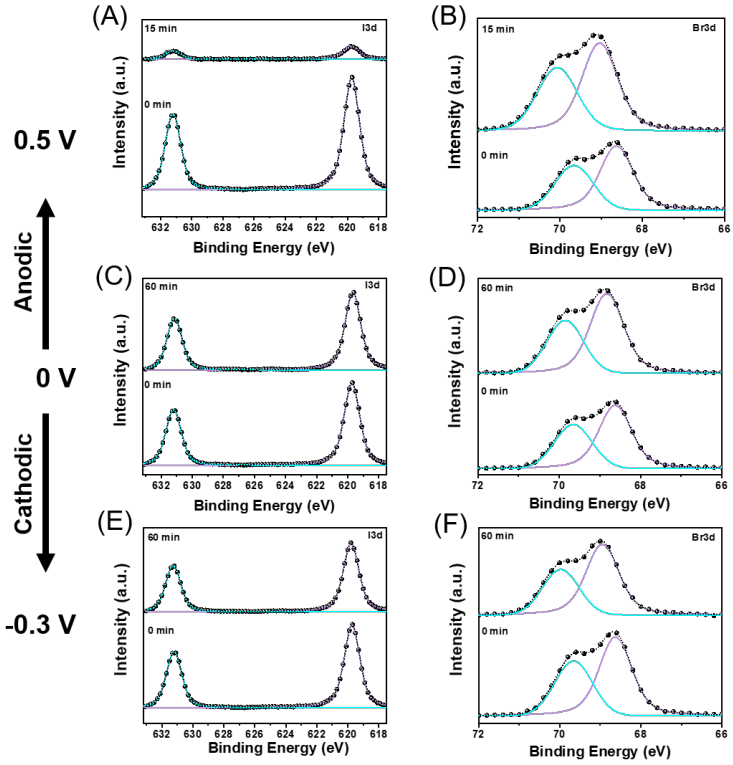

Figure S13: XPS spectra of $MAPbBr_{1.5}I_{1.5}$ films before and after the iodide expulsion process. (A,B) I3d and Br3d spectra before/after iodide expulsion at 0.5 V *vs.* Ag/AgCl. (C,D) I3d and Br3d spectra before/after iodide expulsion at 0 V *vs.* Ag/AgCl. (E,F) I3d and Br3d spectra before/after iodide expulsion at -0.3 V *vs.* Ag/AgCl. From analysis of these peaks the ratio of bromide to iodide ions on the surface was determined (Table S3). Iodide expulsion was induced using 405 nm CW irradiation (50 mW/cm^2) under the same conditions described in the main text.

Table S3: Summarized results of XPS analysis. The ratio of the halide ions (Br and I) before/after iodide expulsion is given. The "0 minute" timepoint for each sample was taken from the same film, as each film was from the same batch synthesized on the same day.

Sample	Irradiation Time	I %	Br %	Standard Deviation
$MAPb(Br_{1.5}I_{1.5})$ @ 0.5 V vs. Ag/AgCl	**0 min**	51.55	48.45	0.75
	15 min	13.30	86.70	5.5
$MAPb(Br_{1.5}I_{1.5})$ @ 0 V vs. Ag/AgCl	**0 min**	51.55	48.45	0.75
	60 min	44.55	55.45	1.45
$MAPb(Br_{1.5}I_{1.5})$ @ -0.3 V vs. Ag/AgCl	**0 min**	51.55	48.45	0.75
	60 min	50.85	49.10	0.65

3. References:

(1): Samu, G. F.; Scheidt, R. A.; Kamat, P.V.; Janáky, C. Electrochemistry and Spectroelectrochemistry of Lead Halide Perovskite Films: Materials Science Aspects and Boundary Conditions. *Chem. Mater.* **2018**, *30*, 561–569.

(2): Scheidt, R. A.; Samu, G. F.; Kamat, P.V.; Janáky, C. Modulation of Charge Recombination in $CsPbBr_3$ Perovskite Films with Electrochemical Bias. *J. Am. Chem. Soc.* **2018**, *140*, 86–89.

(3): Samu, G. F.; Balog, Á.; De Angelis, F.; Meggiolaro, D.; Kamat, P. V.; Janaky, C. Electrochemical Hole Injection Selectively Expels Iodide from Mixed Halide Perovskite Films. *JACS*. **2019**, *141*, 10812–10820.

(4): Chen, S.; Goh, T. W.; Sabba, D.; Chua, J.; Mathews, N.; Huan, C. H. A.; Sum, T. C. Energy Level Alignment at the Methylammonium Lead Iodide/copper Phthalocyanine Interface. *APL Mater.* **2014**, *2*, 081512/1−081512/7.

(5): Mathew, P. S.; Samu, G. F.; Janaky, C.; Kamat, P. V. Iodine (I) Expulsion at Photoirradiated Mixed Halide Perovskite Interface. *Should I Stay or Should I Go? ACS Energy Lett.* **2020**, *5*, 1872–1880,

(6): Li, X.; Reynal, A.; Barnes, P.; Humphry-Baker, R.; Zakeeruddin, S. M.; De Angelis, F.; O'Regan, B. C. Measured Binding Coefficients for Iodine and Ruthenium Dyes; Implications for Recombination in Dye Sensitised Solar Cells. *Phys. Chem. Chem. Phys*. **2012**, *14*, 15421–15428.

(7): Kim, G. Y.; Senocrate, A.; Yang, T.-Y.; Gregori, G.; Grätzel, M.; Maier, J. Large tunable photoeffect on ion conduction in halide perovskites and implications for photodecomposition, *Nat. Mater.* **2018,** *17*, 445-449.